
Article:
Ran, Z. orcid.org/0009-0004-8582-2835, Zhu, Z.-Q. orcid.org/0000-0001-7175-3307 and Liang, D. orcid.org/0000-0002-1574-9810 (2025) Comparative study of dual-rotor permanent magnet machines with series and parallel magnetic circuits. World Electric Vehicle Journal, 16 (1). p. 12. ISSN 2032-6653

https://doi.org/10.3390/wevj16010012

World Electric Vehicle Journal

MDPI

Article

Comparative Study of Dual-Rotor Permanent Magnet Machines with Series and Parallel Magnetic Circuits

Zhitong Ran, Zi-Qiang Zhu * and Dawei Liang

Department of Electronic and Electrical Engineering, The University of Sheffield, Sheffield S1 3JD, UK; zran1@sheffield.ac.uk (Z.R.); d.liang@sheffield.ac.uk (D.L.)
* Correspondence: z.q.zhu@sheffield.ac.uk

Abstract: This paper compares the electromagnetic performances of radial-flux, dual-rotor, permanent magnet (DRPM) machines with series (S) and parallel (P) magnetic circuits for two rotors, i.e., SDRPM and PDRPM, accounting for different slot/pole number combinations, stator winding configurations, and machine sizes. The machines are optimized using the finite element analysis (FEA) based on the genetic algorithm. It shows that the PDRPM machine with the tooth coil (TC) configuration has the highest permanent magnet (PM) utilisation compared to the PDRPM with toroidal winding (TW) configuration and the SDRPM machine with the TC configuration under different slot/pole number combinations. The scaling effects of the machine size on the torque have been investigated. The TW-PDRPM machine is suitable for large-radius and short-axial length applications due to the short end-winding length of the TW configuration, while the TC-PDRPM is better for small-radius and long-axial length applications. The TC-SDRPM performs well when both the machine outer radius and axial length increase. Finally, the TC-SDRPM and TW-PDRPM machines are prototyped and validated experimentally.

Keywords: dual rotor; fractional slot; permanent magnet machine; pole number combinations; radial flux; toroidal winding

Academic Editor: Grzegorz Sierpiński

Received: 5 December 2024
Revised: 22 December 2024
Accepted: 25 December 2024
Published: 28 December 2024

Citation: Ran, Z.; Zhu, Z.-Q.; Liang, D. Comparative Study of Dual-Rotor Permanent Magnet Machines with Series and Parallel Magnetic Circuits. *World Electr. Veh. J.* **2025**, *16*, 12. https://doi.org/10.3390/wevj16010012

1. Introduction

Industrial sectors, such as maritime, aviation, electric vehicles, domestic appliances, and crane operations, have increasingly used permanent magnet (PM) machines in recent years. This is because PM machines have high torque density and efficiency [1]. Among different PM machine topologies, the radial-flux rotor PM machine is the most common due to its superior electromagnetic performance, cost-effectiveness, reliability, and ease of manufacturing [2–4].

In different radial-flux rotor PM machine topologies, surface-mounted PM (SPM) machines are widely used due to their simple structure, easy manufacturability, and high air gap flux density [5,6], as shown in Figure 1. To further increase the torque density and efficiency of the conventional radial-flux SPM machine, the radial-flux, dual-rotor SPM (DRSPM) machine is proposed in [7,8], which consists of a single shared sandwiched stator and two rotors. Both rotors have the same pole number and are located on opposite sides of the stator, rotating at the same speed and assembled on the same shaft. In this design, the inner and outer PMs generate the fluxes in parallel through a shared stator yoke. The DRSPM machine with parallel magnetic circuits is denoted as the PDRPM machine in the paper.

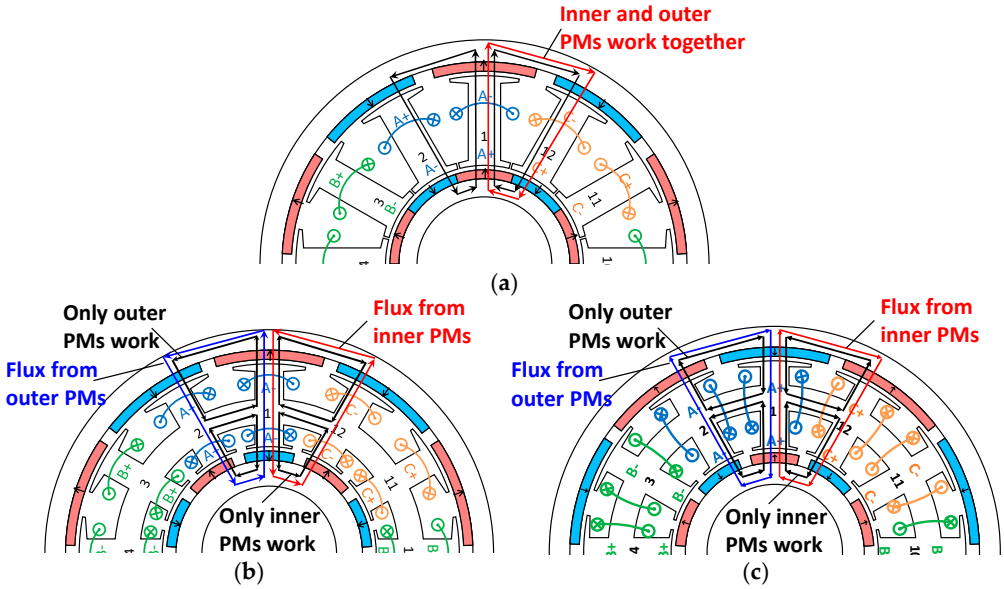

Figure 1. Machine topologies. (**a**) TC−SDRPM. (**b**) TC−PDRPM. (**c**). TW−PDRPM.

In the PDRPM machine (Figure 1b), the inner and outer PMs have opposing polarities of magnetic motive forces (MMF) in the inner and outer air gaps. To produce opposite polarities of the MMFs in different air gaps, the PDRPM machine uses either the toroidal winding (TW) or tooth coil (TC) configurations. The TW configuration allows stator coils to be wound on the common stator yoke directly [9–11]. In contrast, in the TC configuration, stator coils are wound on the inner and outer stator teeth in different directions [12], as shown in Figure 1b,c. The applications of TW- and TC-PDRPM machines to direct-drive wind power generators have been investigated in [13–16], where the active mass, stability, and PM usage of TW-PDRPM machines are analysed in [15], while the performance of TC-PDRPM machines with different slot/pole number combinations is analysed in [16]. In addition, the torque enhancement of both TW- and TC-PDRPM machines by using magnetic field modulation is investigated in [17].

The PDRPM machine combines the features of the internal rotor and external rotor PM machines, since the inner and outer fluxes are in parallel. However, this design requires a shared stator yoke, which leads to increased iron loss and reduced slot areas. To mitigate these issues, a radial-flux yokeless fractional slot (FS) DRSPM machine is proposed in [18], which has the series connection of the inner and outer magnetic circuits, referred to as the SDRPM machine in the paper, as shown in Figure 1a. Compared to PDRPM machines, SDRPM machines have the same flux pattern for both the inner and outer PMs, resulting in the same direction for the fluxes generated by them and the same polarities of the MMFs in the inner and outer air gaps. This approach eliminates the stator yoke, significantly reducing weight and iron loss [19,20]. The yokeless modular stator structure of the SDRPM machine provides a large slot area and allows the stator coil to be wound on the modular stator core directly, which improves the slot fill factor [21,22]; although, the mechanical robustness becomes weaker.

To date, the comparison of the electromagnetic performances of PDRPM and SDRPM machines can only be found in a few papers [23,24]. It has been reported in [23] that the integer slot (IS) TW-PDRPM machines show better performance in megawatt-scale wind power generation applications compared to the IS TC-SDRPM machines, since the TW configuration in the IS TW-PDRPM machines reduces the length of end-windings.

However, this conclusion is only valid for the IS DRPM machines in high-power applications (MW), since in this case, the copper loss and active mass of end-windings

in the IS TC-SDRPM machines are significantly higher than those in the IS TW-PDRPM machines. In contrast, an opposite conclusion can be found in [24] for fractional slot (FS) SDRPM and PDRPM machines in low-power applications. It is shown in [24] that the FS TC-SDRPM machines exhibit higher torque than the FS TC-PDRPM machines, since the yokeless modular structure provides a larger slot area and allows for a higher input current under the same copper loss condition.

Overall, the scopes of the existing papers are summarised in Table 1. As can be seen, the IS and FS PDRPM and/or SDRPM are compared individually based on specific power range. Meanwhile, the effect of different winding configurations is mainly influenced by the slot/pole number combinations, which are not considered.

Table 1. Review of scopes of existing papers.

Machine Type	Slot/Pole Number Combinations			Power Range		
	IS	FS	IS + FS	High	Low	Scaling
TW-PDRPM	[23]	-	√	[23]	[23]	√
TC-PDRPM	-	[24]	√	-	[24]	√
TC-SDRPM	[23]	[24]	√	[23]	[23,24]	√
This paper: √.						

In this context, this paper aims to provide a thorough investigation of different DR-SPM machines, i.e., TC-SDRPM, TC- and TW-PDRPM machines, accounting for various applications, the machine size scaling effect, and slot/pole number combinations. All machines are optimised by the finite element analysis (FEA)-based genetic algorithm to maximise torque production, where the contributions of the inner and outer rotor-to-torque production in all machines are separately analysed. It will be shown that, since the outer rotor PM produces a relatively higher back electromotive force (EMF), the TC-PDRPM machine exhibits the highest PM utilisation. In comparison, the TW-PDRPM machine takes advantage of the short end-winding length of the TW configuration, which allows a higher input current under the same copper loss condition. However, as the number of rotor poles increases, the stator armature reaction is enhanced, and consequently, the optimised TW-PDRPM has a thicker common stator yoke, which occupies the stator slot area and reduces the torque. Besides, this paper investigates the machine size scaling effect on the electromagnetic performance of all machines to consider their feasibilities in different power ranges. It shows that, in terms of torque output, the TW-PDRPM machine is suited for applications with larger radii and shorter axial lengths. Conversely, the TC-PDRPM machine is better for applications with smaller radii and longer axial lengths. When both the radius and axial length are increased, the TC-SDRPM machine performs better.

This paper is organised as follows. Section 2 introduces the topologies of the 12-slot 10-pole (12s10p) TC-SDRPM, TC-, and TW-PDPRM machines. Section 3 describes the global optimisation designs of all machines using the finite element analysis (FEA)-based genetic algorithm. Section 4 compares the electromagnetic performances of all optimised 12s10p machines. Section 5 investigates the influence of the slot/pole number combinations of the TC-SDRPM, TC-, and TW-PDRPM machines. The influence of scaling machine sizes on the machine performance is studied in Section 6. Section 7 provides the experiment results, and Section 8 concludes this paper.

2. Machine Topologies

The DRPM machines, i.e., TC-SDRPM, TC-PDRPM, and TW-PDRPM, are investigated based on the 12s10p combination firstly, as shown in Figure 2, since 12s10p has lower cogging torque and better electromagnetic performance than other slot/pole number

combinations [25,26]. The influence of different slot/pole number combinations will be investigated later in Section 5.

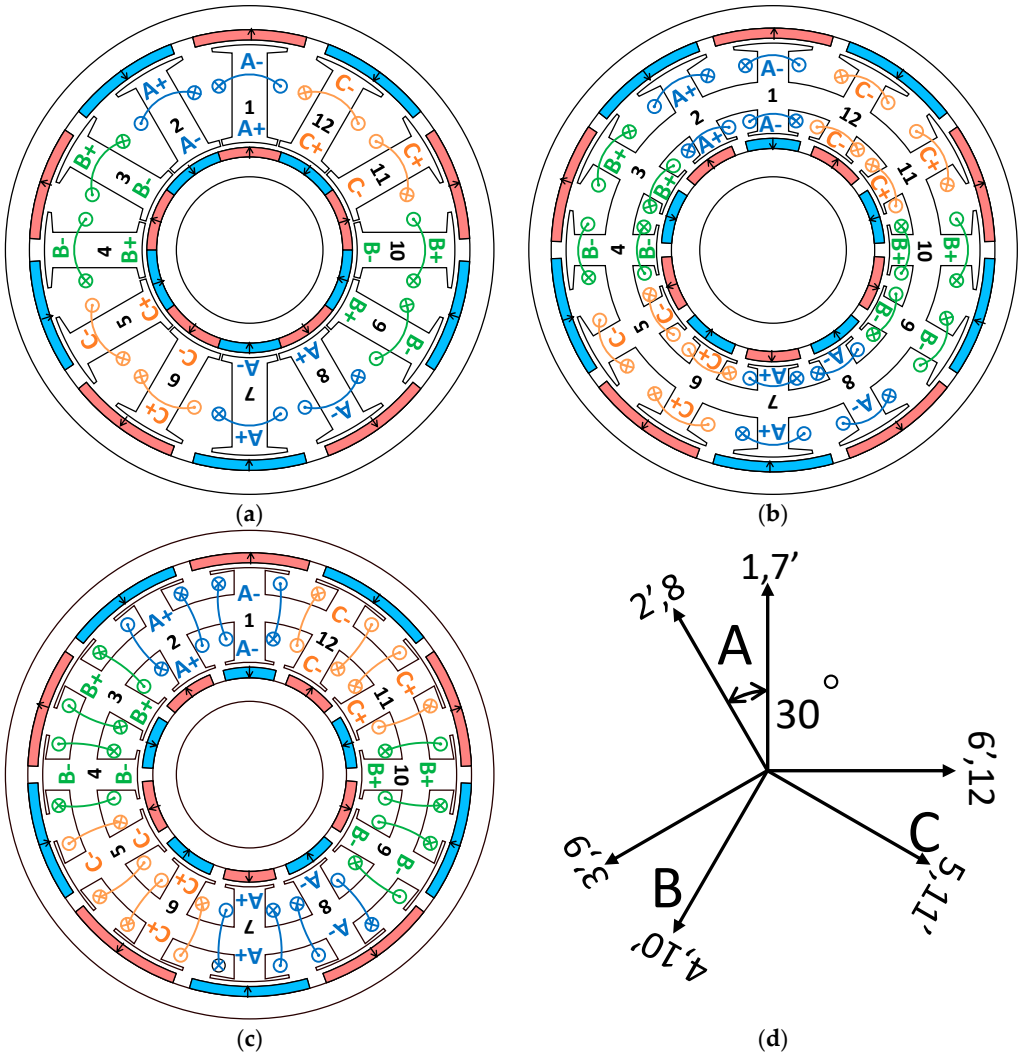

Figure 2. Cross sections of 12s10p machines and coil EMF phasors. (**a**) TC-SDRPM. (**b**) TC-PDRPM. (**c**) TW-PDRPM. (**d**) Coil EMF phasors.

Specifically, the TC-SDRPM machine features a sandwiched yokeless modular stator. The magnetic poles of two rotors are aligned and have the same pole numbers and magnetisation polarities. Therefore, the inner and outer PMs generate the fluxes in series. Secondly, in the TC-PDRPM machine, the inner and outer stator slot areas may differ due to the TC configuration. Thus, under the fixed number of turns per phase condition, the number of turns of the stator winding split wound on the inner and outer stator teeth may differ, according to the corresponding stator slot areas. Thirdly, in the TW-PDRPM machine, the TW configuration is directly wound to the stator windings on the common stator yoke, and thus, it has the same number of turns in the inner and outer slots. In this case, it is preferable that the inner and outer stator slot areas of the TW-PDRPM machine are the same.

3. Optimised Designs

All machines are globally optimised by utilising an FEA-based genetic algorithm in Ansys Maxwell to achieve maximum torque. For a fair comparison, all machines have been designed using the same materials, the same series number of turns per phase of 192, and

the same copper loss of 30 W. The PM volumes of all machines have no restrictions during optimisation to achieve maximum torque for various topologies. Meanwhile, all machines also have the same outer radius and stack length, as listed in Table 2.

Table 2. Design specifications of TC-SDRPM, TC-, and TW-PDRPM machines.

Parameter	Value	Parameter	Value
Outer radius of machine	50 mm	Stack length	50 mm
PM remanence	1.2 T	PM relative permeability	1.05
Number of stator slots	12	Turns per phase	192
Silicon steel lamination grade	M300	NdFeB PM grade	N35SH

Figure 3 shows all the variables involved in the optimisation process, as listed in Table 3. During optimisation, the R_3 and R_4 are varied with inner and outer split ratios. In PDRPM machines, the inner and outer fluxes are in parallel. Therefore, the stator tooth widths of the inner and outer parts can differ in the optimised design of PDRPM machines. Additionally, the end-winding is considered during the optimisation. The end-winding configurations are illustrated in Figure 4. To simplify the calculation of the end-winding length, the end-winding length is determined as a semicircle with a diameter equivalent to the length of the "Arc" [27]. Thus, the end-winding length of the TC-SDRPM and TC-PDRPM machines $l_{TC\text{-}end}$ in Figure 4b can be calculated as:

$$l_{TC\text{-}end(y=1,3,5)} = \frac{\pi}{2}\left(\frac{(2y-1)(R_3+h_{is}+R_4-h_{os})}{2N_s}+\frac{w_{st}}{2}\right)+2l_{ex} \quad (1)$$

where y is the coil pitch, N_s is the number of stator slots, R_3 and R_4 are the stator inner and outer radii, respectively, h_{is} and h_{os} are the stator inner and outer tooth–tip height, w_{st} is the tooth width, and l_{ex} is the extend part, as shown in Figure 4a.

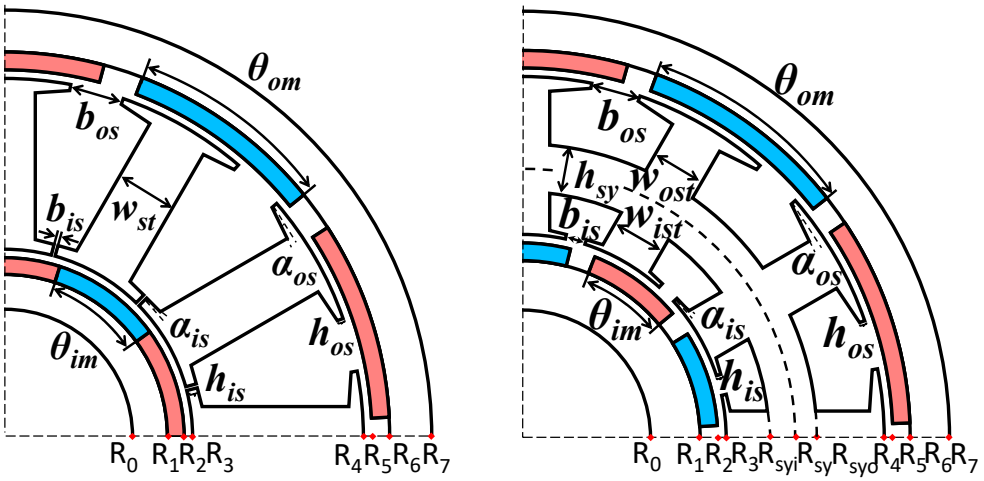

Figure 3. Optimised variables. (**a**) SDRPM. (**b**) PDRPM.

The end-winding length of the TW-PDRPM machine $l_{TW\text{-}end}$ in Figure 4c can be calculated as [28]:

$$l_{TW\text{-}end} = \frac{\pi}{2}\left(\frac{(R_{syi}-R_3-h_{it}+R_4-R_{syo}-h_{os})}{2}+R_{syo}-R_{syi}\right)+2l_{ex} \quad (2)$$

where R_{syi} and R_{syo} are the stator yoke inner and outer radii, respectively.

Table 3. Optimised parameters of 12s10p machines.

Parameters	Symbols	TC-SDRPM	TC-PDRPM	TW-PDRPM
Stator yoke position	R_s/R_7	-	0.51	0.67
Stator yoke height (mm)	h_{sy}	-	5.7	5.8
Stator tooth width (mm)	w_{ist}/w_{ost}	7	7/6.5	6.5/6.3
Outer split ratio	R_4/R_7	0.84	0.83	0.86
Outer slot opening (mm)	b_{os}	6	6.6	8.8
Outer tooth-tip thickness (mm)	h_{os}	1	1	1.1
Outer tooth-tip slope (deg.)	α_{os}	15	11	10
Outer PM thickness (mm)	R_6–R_5	2.0	2.3	1.6
Outer PM pole arc (elec.)	θ_{om}	150	155	161
Outer PM volume (cm^3)	V_{om}	23.9	27	20.5
Inner split ratio	R_2/R_7	0.42	0.39	0.42
Inner slot opening (mm)	b_{is}	0.4	2.4	2.4
Inner tooth-tip thickness (mm)	h_{is}	1	1	1
Inner tooth-tip slope (deg.)	α_{is}	0	6	5.4
Inner PM thickness (mm)	R_2–R_1	2.0	1.7	2.4
Inner PM pole arc (°elec.)	θ_{im}	180	142	180
Inner PM volume (cm^3)	V_{im}	12.1	7.9	14.8
Total PM volume (cm^3)	V_m	36	34.9	35.3
Input current amplitude (A)	I_{amp}	5.1	5	4.8

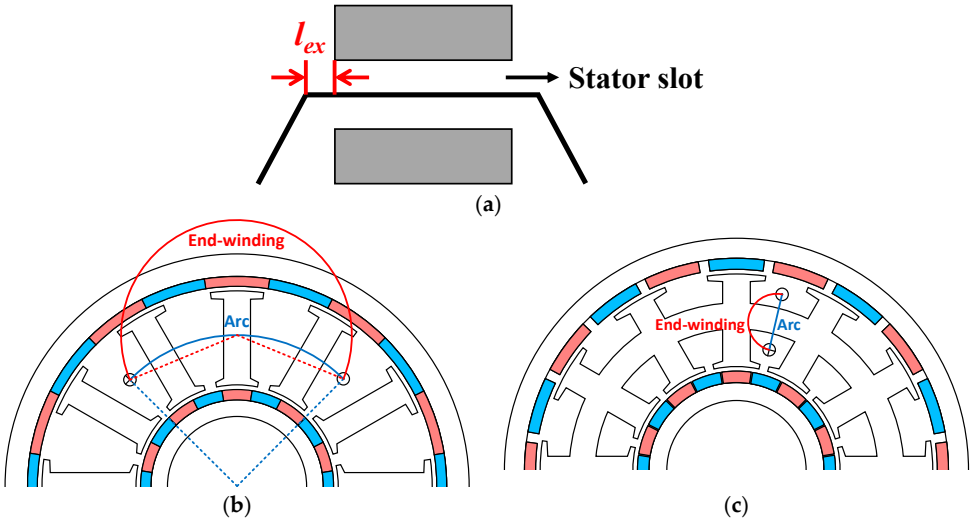

Figure 4. End-winding configuration. (**a**) Side view. (**b**) TC. (**c**) TW.

4. Comparison of Electromagnetic Performances of TC-SDRPM, TC-, and TW-PDRPM Machines

This section compares the electromagnetic performances of the optimised 12s10p TC-SDRPM, TC-, and TW-PDRPM machines by FEA, including air gap flux density, open-circuit flux linkage, back EMF, electromagnetic torque, PM utilisation, overload capability, losses, and efficiency.

4.1. Air Gap Flux Density

Figure 5 shows the open circuit flux lines and magnetic flux density distributions of all optimised 12s10p machines. Since the TC-PDRPM machine has no restriction on the inner and outer slot areas, the optimised stator yoke position is located towards the bottom of the stator teeth. The outer rotor of the TC-PDRPM machine is the main output component, and there is almost no stator winding linking with the flux generated by the inner rotor

PM. In contrast, the TW-PDRPM machine restricts the inner and outer stator slot areas to be equal, and the number of turns of the stator winding in the inner and outer stator slots are the same. For the SDRPM machine, the fluxes generated by the PMs on the inner and outer rotors are in series, and the resultant flux flows through the inner and outer rotors and the yokeless modular stator.

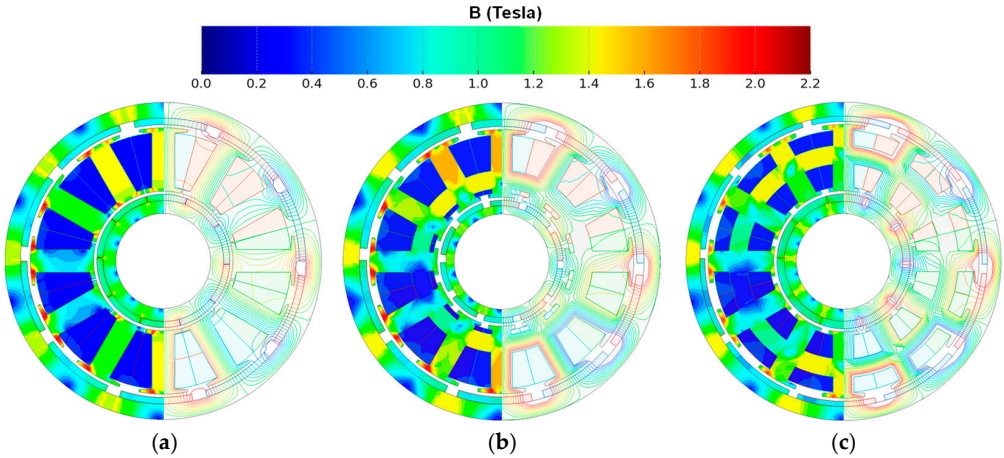

Figure 5. Open circuit flux density and equal potential distributions of optimised 12s10p machines. (**a**) TC-SDRPM. (**b**). TC-PDRPM. (**c**). TW-PDRPM.

Figure 6 shows the inner and outer air gap flux densities of optimised 12s10p machines. In the PDRPM machine, the inner and outer air gap flux densities are relatively separated, because the inner and outer fluxes are in parallel. However, in the SDRPM machine, the inner and outer PMs interact due to the inner and outer fluxes in series. Since its outer rotor inherently has a larger radius than the inner rotor, the outer PM usually generates higher fluxes than the inner PM. Consequently, the inner flux is increased by the higher flux from the outer PMs, resulting in an increased resultant flux in the inner air gap in the SDRPM machine. Thus, the inner air gap flux density in the TC-SDRPM machine is higher than those of the TC- and TW-PDRPM machines.

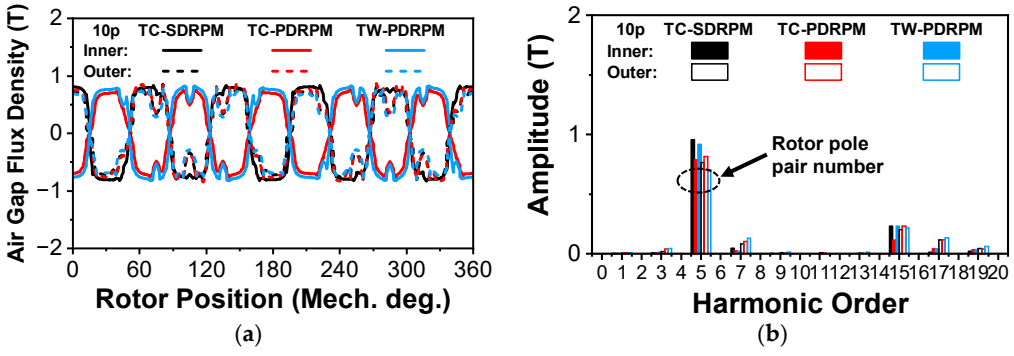

Figure 6. Inner and outer air gap flux densities of 12s10p machines. (**a**) Waveforms. (**b**) Spectra.

As aforementioned, the outer rotor is the main component for producing torque in the TC-PDRPM machine, and thus, outer PM volume in the optimised TC-PDRPM machine is larger than that of the TW-PDRPM and TC-SDRPM machines. Consequently, the outer air gap flux density of the TC-PDRPM machine is the highest among all machines.

4.2. Flux Linkages and Back EMFs

The flux linkage ψ can be calculated as:

$$\psi = N \cdot \Phi \tag{3}$$

where N is the number of turns of the corresponding stator winding, and Φ is the magnetic flux passing through the coil.

Figure 7 shows the open circuit flux lines linked with phase A stator winding of optimised 12s10p machines. The corresponding rotor position at 0 deg is the maximum point of the phase A flux linkage. As can be seen, the outer flux is larger than the inner flux due to the radial structure, and the inner stator winding of the TC-PDRPM machine is almost negligible. In contrast, the number of turns of the inner and outer stator windings of the PDRPM machine with TW configuration must be restricted to be the same.

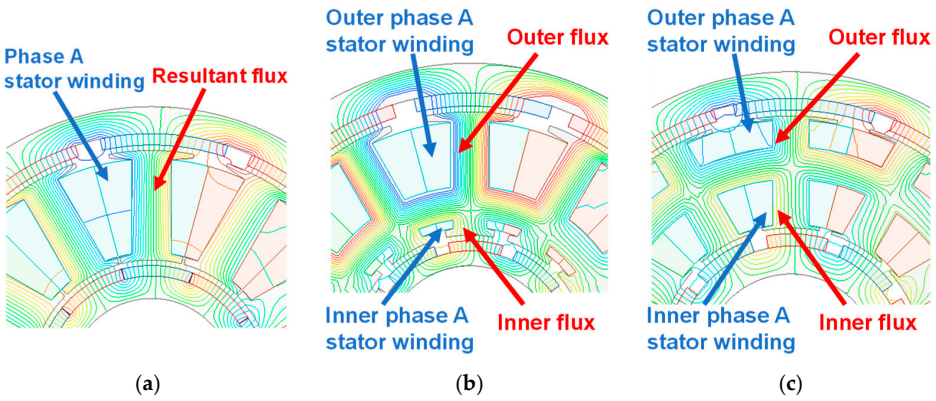

Figure 7. Open circuit flux line linked with phase A stator winding of optimised 12s10p machines (rotor position at 0 deg). (**a**) TC-SDRPM. (**b**). TC-PDRPM. (**c**). TW-PDRPM.

The flux linkages and back EMFs of the optimised 12s10p machines are shown in Figures 8 and 9, respectively. Based on (3), as the number of turns of the inner stator winding of the TC-PDRPM machine is negligible, the flux linkage generated by the inner rotor is almost zero. Therefore, the flux linkage generated by the outer rotor is the main component of total flux linkage in the TC-PDRPM machine. Since the outer flux is larger than the inner flux, the total flux linkage of the TC-PDRPM machine is the highest.

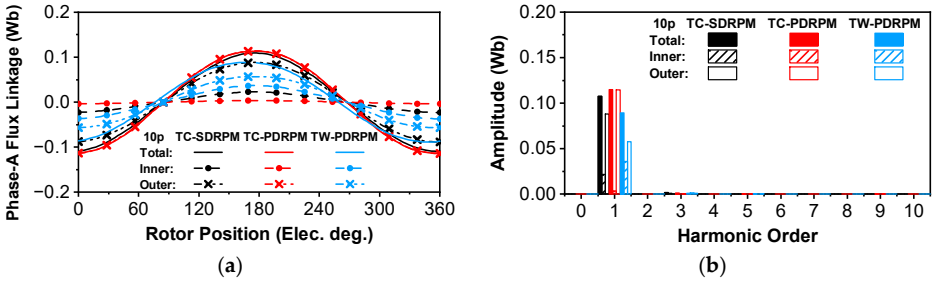

Figure 8. Phase A flux linkages of 12s10p machines. (**a**) Waveforms. (**b**) Spectra.

The TW configuration restricts the number of inner and outer stator winding turns in the PDRPM machine. As a result, the inner rotor of the TW-PDRPM machine produces the highest flux linkage compared to other machines. Conversely, the outer rotor of the TW-PDRPM machine generates the lowest flux linkage (Figure 8) due to the outer number of turns also being restricted by the TW configuration, which makes the total flux linkage of the TW-PDRPM machine the lowest. In the TC-SDRPM machine, the inner flux is

detrimental to the outer flux, which lowers the total flux linkage of the TC-SDRPM machine compared to the TC-PDRPM machine. The back EMFs of optimised 12s10p machines have similar trends as the flux linkages, as shown in Figure 9.

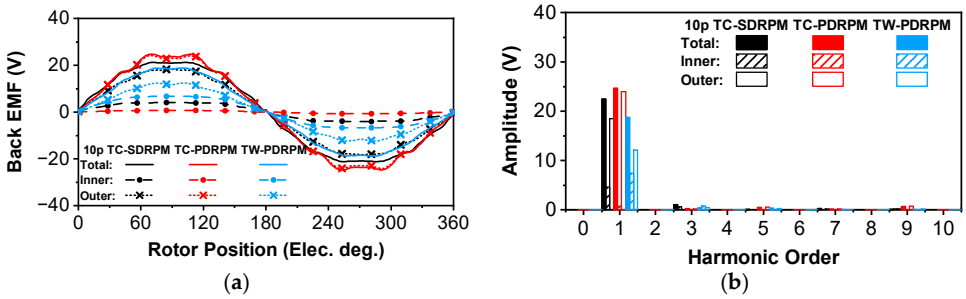

Figure 9. Phase A back EMFs of 12s10p machines (rated speed = 400 r/min). (**a**) Waveforms. (**b**) Spectra.

4.3. Torque, PM Utilisation, and Overload Capability

The on-load torques of all optimised 12s10p machines under 30 W copper loss with zero d axis current control are shown in Figure 10. The TC-PDRPM machine has the highest torque of 4.3 Nm due to its highest back EMF. In contrast, the TW-PDRPM machine has the lowest torque of 3.2 Nm. It can be explained that the TW-PDRPM has the lowest back EMF, and the stator yoke design in the PDRPM machines further reduces the slot area compared with the yokeless structure of the TC-SDRPM machine, leading to an even lower input current in the PDRPM machines with the same copper loss (see Table 3).

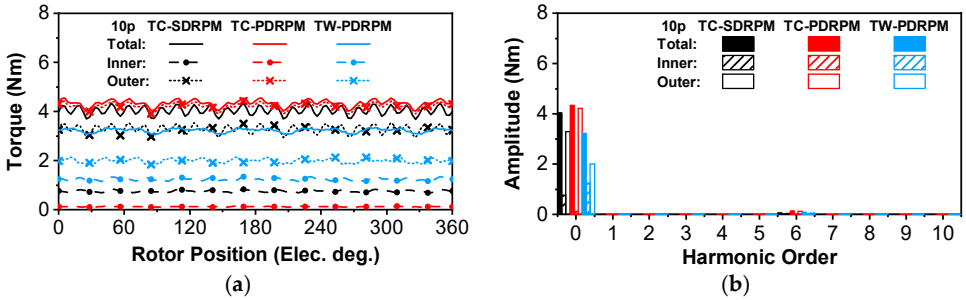

Figure 10. Torques of 12s10p machines. (**a**) Waveforms. (**b**) Spectra.

For maximum torque production for all three machines, their respective PM usage will be different, as presented in Figure 11. In this paper, the PM utilisation $\rho_{\text{Torque/PM}}$ is defined as the ratio of average torque to PM volume, i.e.,

$$\rho_{\text{Torque/PM}} = \frac{T_{\text{avg}}}{V_{\text{PM}}} \tag{4}$$

where T_{avg} is the average torque, and V_{PM} is the PM volume. It can be seen that the TC-PDRPM machine has the highest outer PM utilisation, while the TW-PDRPM machine has the highest inner PM utilisation.

The overload capabilities of all 12s10p machines are shown in Figure 12. It can be seen that the TC-SDRPM and TC-PDRPM machines have the same overload capabilities. However, the TC-PDRPM machine always produces higher torque than the TC-SDRPM machine at different copper losses. In contrast, the TW-PDRPM machine has the worst overload capability.

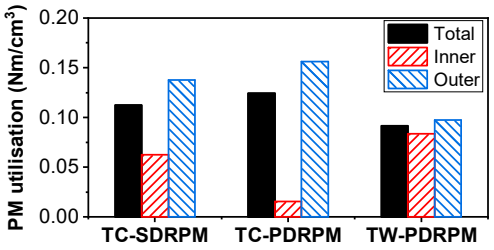

Figure 11. PM utilisations of 12s10p machines.

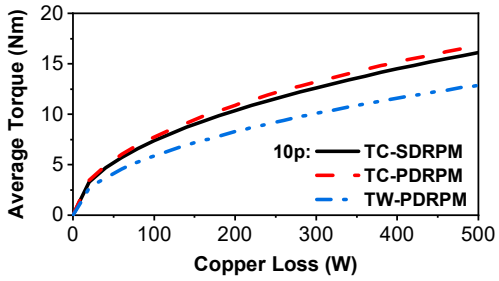

Figure 12. Torques versus copper loss of 12s10p machines.

4.4. Loss and Efficiency

The PM eddy current, iron, and copper losses of all optimised 12s10p machines at the rated load are shown in Figure 13. As can be seen, the TC-SDRPM machine has the lowest iron loss due to its yokeless stator structure.

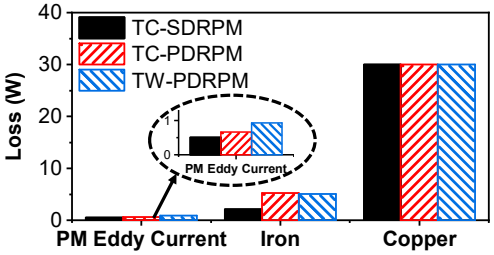

Figure 13. Losses of 12s10p machines (rated speed = 400 r/min).

Furthermore, the efficiencies (5) of all three machines are calculated. The efficiencies of the TC-SDRPM, TC-PDRPM, and TW-PDRPM machines are 98.02%, 97.98%, and 97.29%, respectively. Clearly, the 12s10p TC-SDRPM machine has the highest efficiency due to the low PM eddy current and iron losses.

$$\eta = \frac{T_{\text{avg}}\omega}{T_{\text{avg}}\omega + P_{\text{loss}}} \tag{5}$$

where ω is the machine rotating speed, and P_{loss} is the total loss in the machine. The performances of the 12s10p TC-SDRPM, TC-PDRPM, and TW-PDRPM machines are summarised in Table 4.

Table 4. Performances of 12s10p TC-SDRPM, TC-PDRPM, and TW-PDRPM machines.

Performances	TC-SDRPM	TC-PDRPM	TW-PDRPM
Torque (Nm)	4.0	4.3	3.2
PM utilisation (Nm/cm^3)	0.111	0.123	0.091
Loss (W)	32.3	35.5	35.7
Efficiency (%)	98.02	97.98	97.29

5. Influence of Slot/Pole Number Combinations of TC-SDRPM, TC-, and TW-PDRPM Machines

The influence of the slot/pole number combinations of TC-SDRPM, TC-PDRPM, and TW-PDRPM machines are investigated in this section, i.e., 12s10p FS machines, 12 slots 20 poles (12s20p), and 12 slots 22 poles (12s22p) IS machines. Their winding connections and corresponding coil EMF phasors are shown in Figure 14.

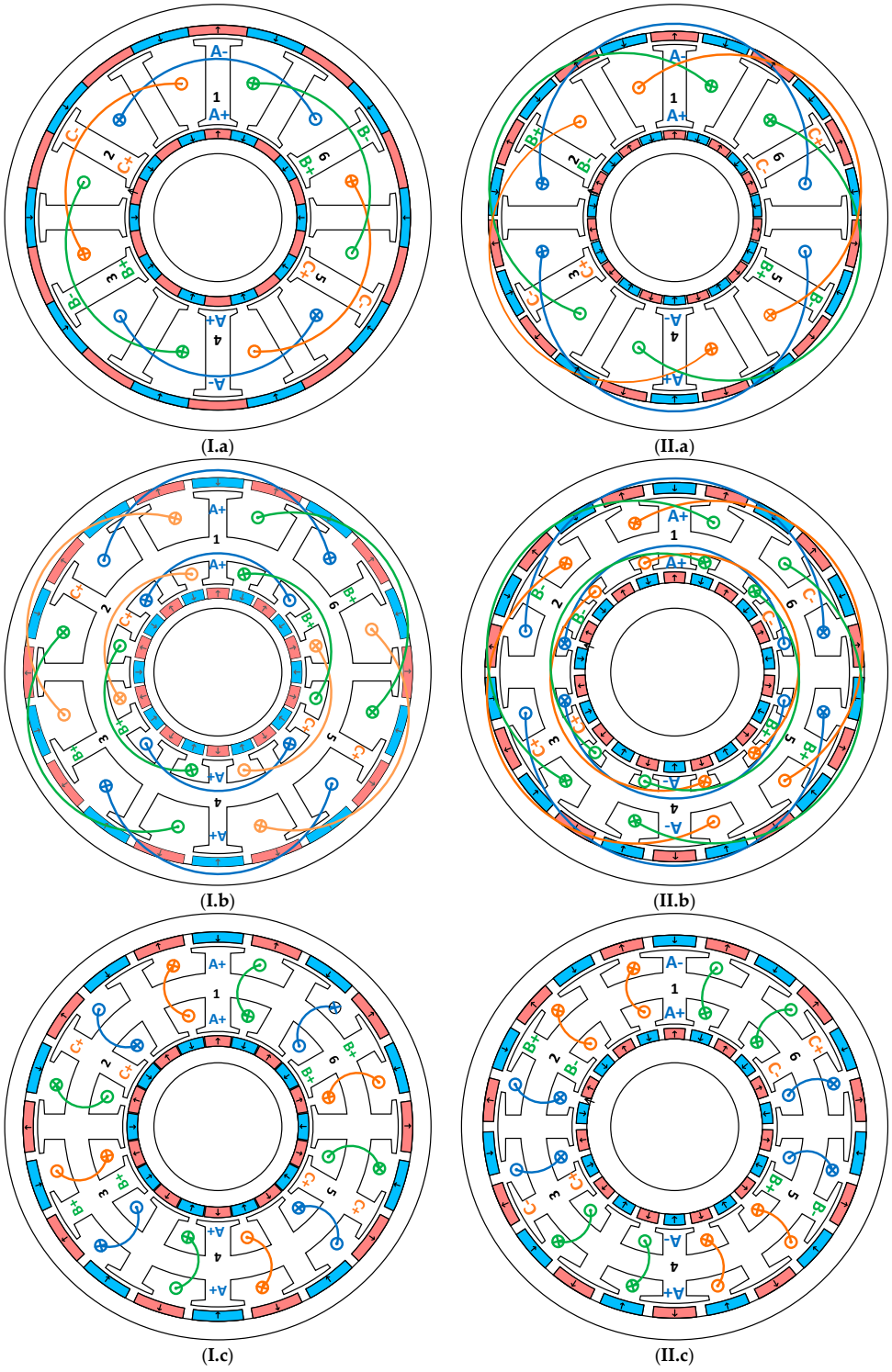

Figure 14. *Cont.*

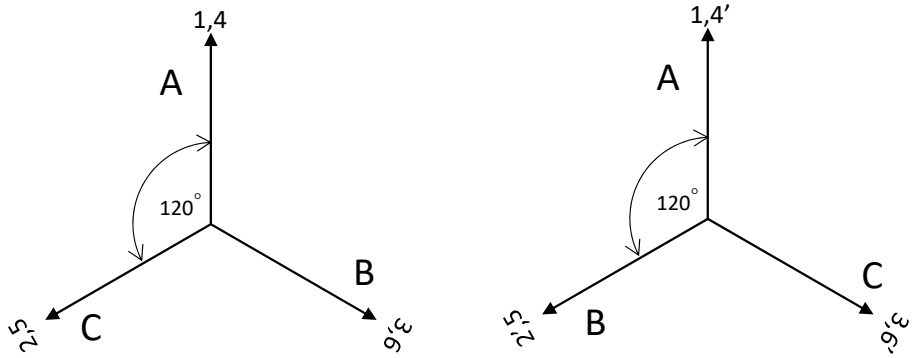

(**I.d**) (**II.d**)

Figure 14. Cross-sections of machines with different slot/pole number combinations and corresponding coil EMF phasors. (**I**). 12s20p. (**II**). 12s22p (**a**) TC-SDRPM. (**b**) TC-PDRPM. (**c**) TW-PDRPM. (**d**) Corresponding coil EMF phasors.

The number of slots per pole per phase q can be calculated by:

$$q = \frac{N_s}{2mp} \tag{6}$$

where N_s is the number of the stator slot; m is the number of the phase; p is the number of the rotor pole pairs. It should be noted that the pole pair numbers of the 12s20p and 12s22p combinations in (6) are the pole pair numbers of the armature windings as 2 and 1, respectively. Thus, the q of the 12s10p machines is 2/5. The q of the 12s20p and 12s22p IS machines are 1 and 2, respectively.

For all machines with different slot/pole number combinations, the windings are connected for the highest winding factors. Therefore, the optimal coil pitches of 12s10p, 12s20p, and 12s22p SDRPM machines are 1, 3, and 5, respectively. All machines with different slot/pole number combinations are globally optimised with the same condition as Section 3 to maximise the torque. The optimised parameters are listed in Table 5.

Table 5. Parameters of optimised of TC-SDRPM, TC-, and TW-PDRPM machines with different slot/pole number combinations.

Parameters	Symbols	TC-SDRPM		TC-PDRPM		TW-PDRPM	
Slot/pole number combination	N_s/p	12/20	12/22	12/20	12/22	12/20	12/22
Stator tooth width (mm)	w_{ist}/w_{ost}	3.8	4	2/4.2	2.4/4.8	2.7/5.3	2.6/5.6
Stator yoke position	R_s/R_7	-	-	0.51	0.55	0.66	0.67
Stator yoke height (mm)	h_{sy}	-	-	5.6	6.4	5.7	6
Inner split ratio	R_2/R_7	0.41	0.42	0.38	0.4	0.45	0.47
Outer split ratio	R_4/R_7	0.86	0.83	0.85	0.82	0.85	0.84
Inner slot opening (mm)	b_{is}	3.2	3.7	5.3	6.2	6	4
Outer slot opening (mm)	b_{os}	10.4	12.3	12.8	8.2	9.4	5.2
Inner tooth-tip thickness (mm)	h_{is}	1	1.3	1.3	1.5	1	1
Outer tooth-tip thickness (mm)	h_{os}	1.3	1.1	1.2	1.1	1	1
Inner tooth-tip slope (deg.)	α_{is}	15	6.1	9.5	15	9.7	5
Outer tooth-tip slope (deg.)	α_{os}	17	12.7	10.5	10	12	11.4
Inner PM thickness (mm)	R_2–R_1	2.2	1.9	2.3	1.9	2.2	2.2
Outer PM thickness (mm)	R_6–R_5	2.3	2	2	1.9	2.1	2.3
Inner PM pole arc (°elec.)	θ_{im}	180	164	15.3	15.4	17.2	14.2
Outer PM pole arc (°elec.)	θ_{om}	180	163	16.5	11.9	15.2	11.8
Inner PM volume (cm^3)	V_{im}	13.4	11.2	11.1	10.7	14.5	13.7
Outer PM volume (cm^3)	V_{om}	31.9	25.9	26	19.1	25	22.7
Total PM volume (cm^3)	V_{PM}	45.3	37.1	37.1	29.8	39.5	36.4
Input current amplitude (A)	I_{amp}	5.3	3.8	4.7	3.5	4.9	4.5

5.1. Air Gap Flux Density

Figure 15 shows the open circuit flux lines and magnetic flux density distributions of all optimised machines. With the increase in the pole number, the pole pitch decreases, and the magnetic saturations on the stator and rotor are less.

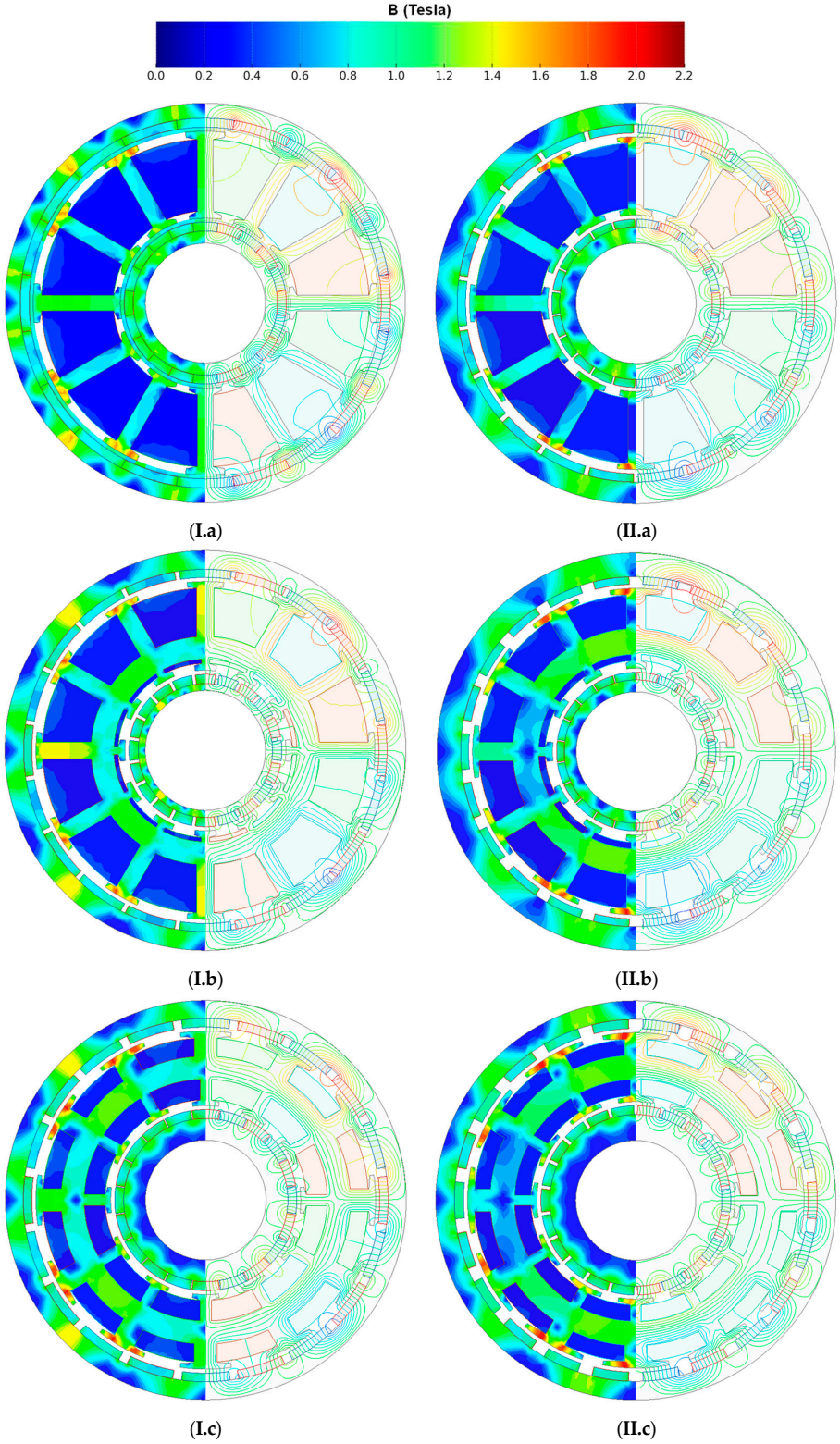

Figure 15. Open circuit flux density and equal potential distributions of optimised machines with different slot/pole number combinations. (**I**). 12s20p. (**II**). 12s22p (**a**) TC-SDRPM. (**b**) TC-PDRPM. (**c**) TW-PDRPM.

Figure 16 shows the variations in the inner and outer air gap flux densities of all machines with pole numbers. In the TC-SDRPM machine, the interaction between inner and outer fluxes decreases the outer air gap flux density, as the inner air gap flux density decreases with the pole number. As mentioned in Section 4, the inner rotor contributes minimally to the TC-PDRPM machine. Therefore, the TC-PDRPM machine exhibits the lowest inner air gap flux density.

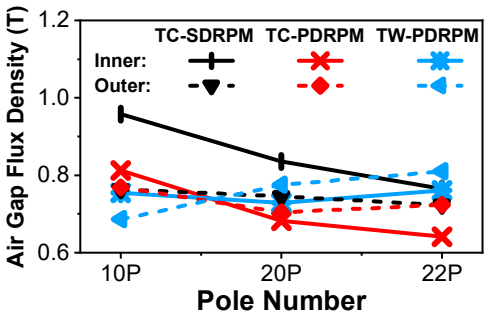

Figure 16. Inner and outer air gaps flux densities versus pole numbers.

5.2. Flux Llinkages and Back EMFs

Figure 17 shows the phase A flux linkages of all machines with different pole numbers. In TC-PDRPM machines with different pole numbers, the flux linkage generated by the inner rotor is negligible. However, the outer rotor radius is significantly larger than that of the inner rotor, and the outer PM generates higher flux due to the larger PM width. As a result, the outer rotor generates significantly higher flux linkage. Thus, TC-PDRPM machines with different slot/pole number combinations have the highest total flux linkages among all machines. The total flux linkages of the 10p and 22p TC-SDRPM machines are higher than those of the corresponding TW-PDRPM machines. The outer flux linkages of the 20p TW-PDRPM and TC-SDRPM machines are similar. However, the TC-SDRPM machine has a lower inner flux linkage compared to the TW-PDRPM machine. Therefore, the total flux linkage of the 20p TW-PDRPM machine is higher than that of the 20p TC-SDRPM machine. The back EMFs and flux linkages of all machines under different pole numbers with similar relationships are shown in Figure 18.

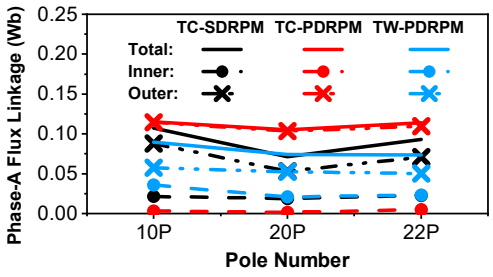

Figure 17. Phase A flux linkages versus pole numbers.

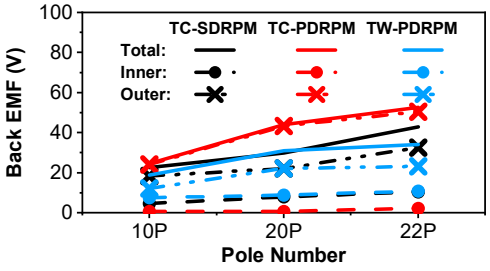

Figure 18. Back EMFs versus pole numbers (rated speed = 400 r/min).

5.3. Torque, PM Utilisation, and Overload Capability

The torques and PM utilisations of TC-SDRPM, TC-, and TW-PDRPM machines with different numbers of slot/pole number combinations are shown in Figures 19 and 20, respectively.

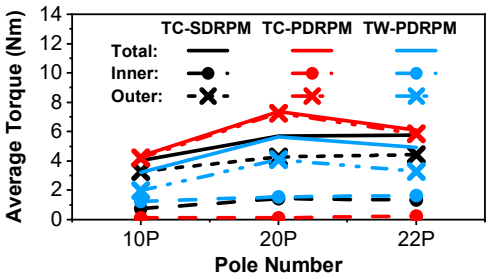

Figure 19. Torques versus pole numbers.

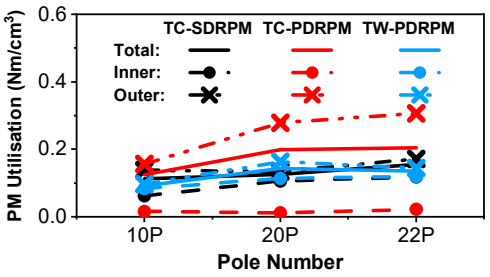

Figure 20. PM utilisations versus pole numbers.

The TC-PDRPM machines with different slot/pole number combinations and different winding configurations exhibit the highest torque due to their highest back EMF. Moreover, the total PM utilisations of the TC-PDRPM machines are higher than other types of machines. On the other hand, the torques of TW-PDRPM machines with different slot/pole number combinations are the lowest. Although the TW configuration has a shorter end-winding length than the TC configuration, the yokeless modular stator structure provides a larger slot area for the TC-SDRPM machines. The 10p and 20p TC-SDRPM machines allow a higher input current than the TW-PDRPM machines, even when considering the end-winding length under the same copper loss condition. For the 22p machines, the TC-SDRPM machine has a higher back EMF than that of the TW-PDRPM machine. Additionally, the 22p machine has a strong 2-pole stator armature reaction. The 22p TW-PDRPM machine faces severe magnetic saturation in the stator yoke, as shown in Figure 21. Therefore, even with a higher input current, the 22p TC-SDRPM machine produces more torque than the 22p TW-PDRPM machine.

Figure 22 shows the average torques of all machines under different copper losses. The machine 22p TW-PDRPM exhibits the weakest overload capability due to the strong armature reaction. On the other hand, the TC-SDRPM machines have a stronger overload capability compared to other types of machines with the same pole number. This is because the series connection of the TC-SDRPM machines leads to almost double the equivalent airgap length, i.e., 2 $\times$ (PM thickness + airgap).

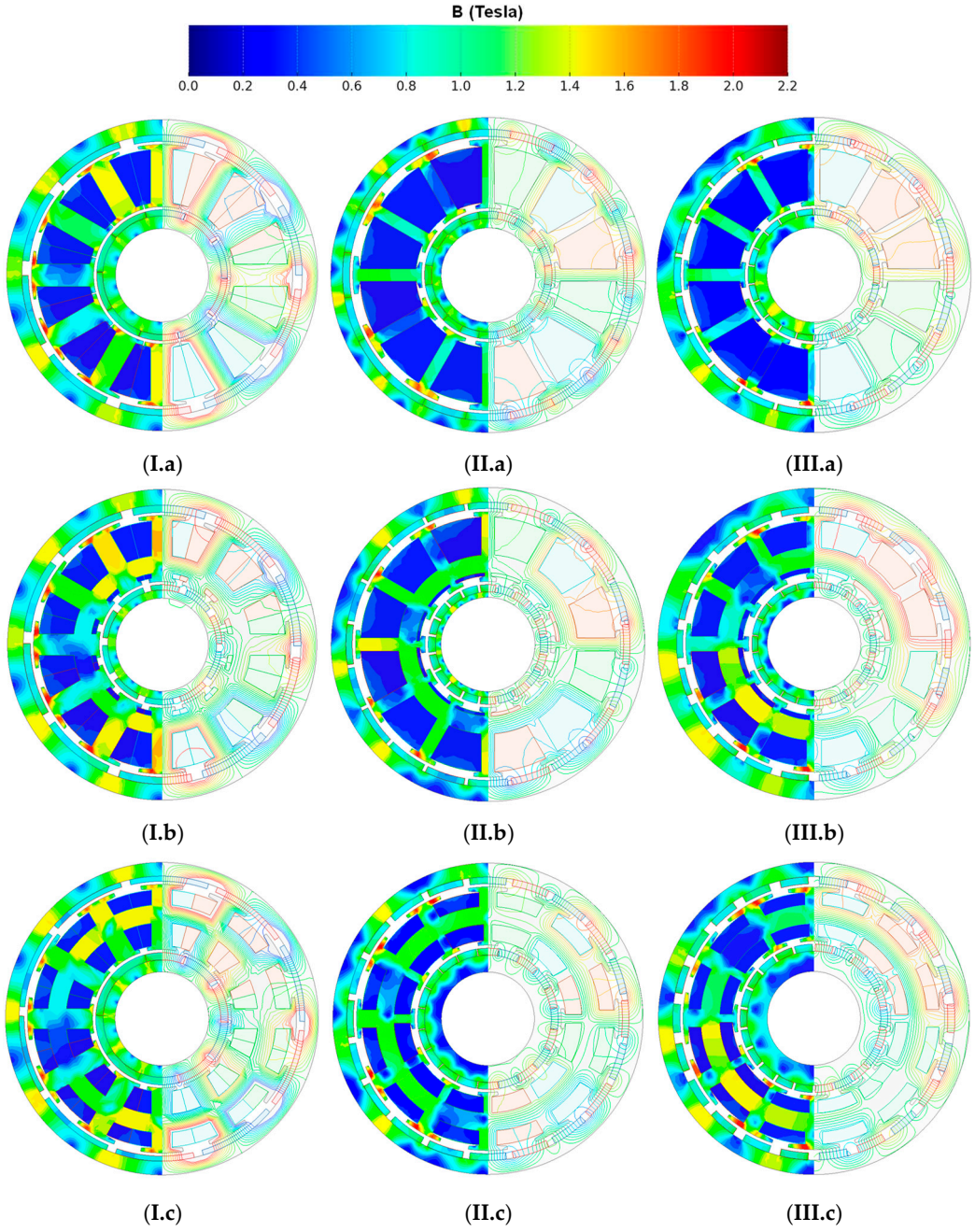

Figure 21. Flux density distributions and flux lines at rated load. (**I**). 12s10p. (**II**). 12s20p. (**III**). 12s22p. (**a**) TC-SDRPM. (**b**) TC-PDRPM. (**c**) TW-PDRPM.

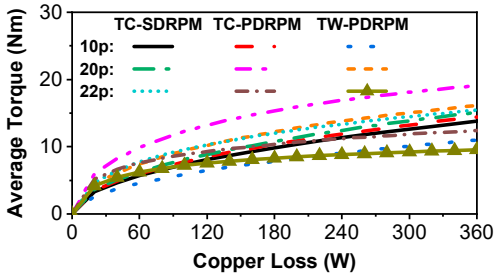

Figure 22. Average torques versus copper loss of TC-SDRPM, TC-, and TW-PDRPM machines with different slot/pole number combinations with zero *d* axis current.

5.4. Loss and Efficiency

The PM eddy current and iron losses of all optimised machines with different slot/pole number combinations are shown in Figure 23. The copper loss for all machines is the same of 30 W. All machines have low iron loss, since they operate at a low speed of 400 r/min. The TC-SDRPM machines have the lowest iron loss with different pole numbers because of the yokeless stator structure. Figure 24 illustrates the efficiencies of all machines. It is observed that all types of machines achieve relatively higher efficiency with the 12s20p slot/pole number combination. The 12s20p TC-PDRPM machine has the highest efficiency compared to all other machines, since it has the highest torque. The performances of the TC-SDRPM, TC-PDRPM, and TW-PDRPM machines with different slot/pole number combinations are summarised in Table 6.

Table 6. Performances of TC-SDRPM, TC-PDRPM, and TW-PDRPM machines with different slot/pole number combinations.

Performances	TC-SDRPM			TC-PDRPM			TW-PDRPM		
Slot/pole	12/10	12/20	12/22	12/10	12/20	12/22	12/10	12/20	12/22
Inner airgap flux density (T)	0.76	0.75	0.72	0.81	0.68	0.64	0.75	0.73	0.76
Outer airgap flux density (T)	0.96	0.84	0.76	0.77	0.7	0.72	0.69	0.78	0.81
Flux linkage (Wb)	0.11	0.07	0.09	0.12	0.11	0.11	0.09	0.07	0.07
Back EMF (V)	22.5	29.8	42.9	24.7	44.1	52.6	18.8	31.0	34.0
Torque (Nm)	4.0	5.4	5.9	4.3	7.2	6.4	3.2	5.4	4.9
PM utilisation (Nm/cm^3)	0.111	0.119	0.159	0.123	0.194	0.210	0.091	0.137	0.132
Loss (W)	32.3	33.8	37.2	35.5	36.5	42.8	35.7	38.2	42.5
Efficiency (%)	98.02	98.46	98.45	97.98	98.75	98.38	97.29	98.26	97.92

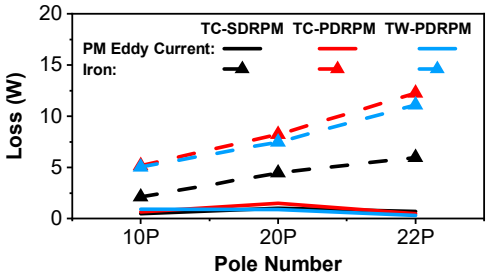

Figure 23. Losses of TC-SDRPM, TC-, and TW-PDRPM machines with different slot/pole number combinations (rated speed = 400 r/min).

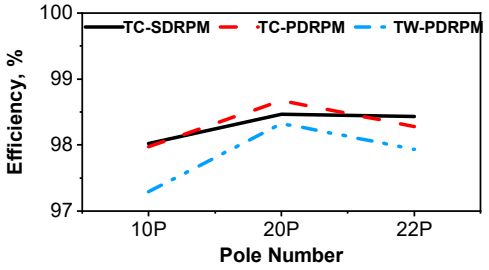

Figure 24. Efficiencies of TC-SDRPM, TC-, and TW-PDRPM machines with different slot/pole number combinations (rated speed = 400 r/min).

6. Influence of Machine Size

According to [23], the IS PDRPM machine outperforms the IS SDRPM machine in megawatt (MW) wind power generation applications. However, different machine sizes with different slot/pole number combinations should be discussed for different applications. Therefore, this section investigates the influence of the machine size for TC-SDRPM and TC-

and TW-PDRPM machines with different slot/pole number combinations. The scaling-up analysis is conducted in three distinct directions, as illustrated in Figure 25. The red arrow K_r presents the machine only scaling up in the radial direction but keeping other parameters the same in the axial direction. The blue arrow K_a shows the machine only scaling up in the axial direction but keeping other parameters the same in the radial direction.

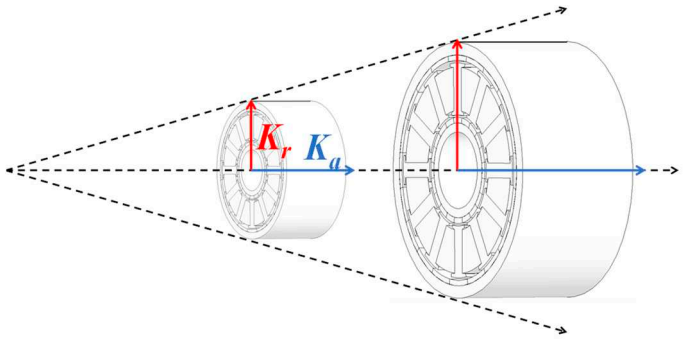

Figure 25. Scale-up method of machine.

6.1. Scale-Up in Radial Direction

In the radial direction, the copper loss scales up as K_r^2. The end-winding length is influenced significantly by the radially scaling up. The stator armature winding input current with zero d axis current control and the torque of all machines varied with the K_r are shown in Figure 26.

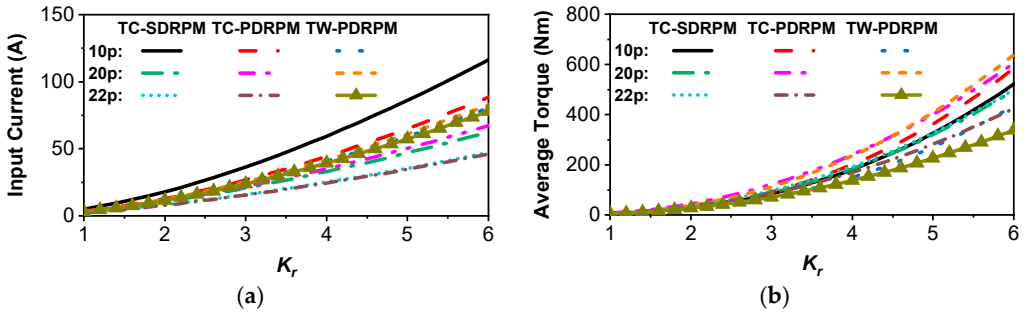

Figure 26. Variation of average torque and stator q axis input current with K_r. (**a**) Input current. (**b**) Average torque.

In this case, the torque of the 12s20p TW-PDRPM machine increases to the highest with the increase in K_r. The IS TW-PDRPM machines have the advantage of shorter end-winding length. Thus, the 12s20p and 12s22p TW-PDRPM machines have a higher input current with increased K_r. However, the strong 2-pole stator armature reaction in the 12s22p TW-PDRPM machine leads to severe magnetic oversaturation, which results in the torque of the 12s22p TW-PDRPM machine increasing slowly with K_r.

6.2. Scale-Up in Axial Direction

In the axial direction, copper loss increases in proportion to K_a. Figure 27 shows the input currents and torques of all machines varying with K_a. With axial scaling, the effect of the end-winding length becomes negligible gradually.

Therefore, the input currents in the TC-SDRPM and TC-PDRPM machines increase more with K_a than in the TW-PDRPM machines. A more significant increase in the torque of the TC-SDRPM and TC-PDRPM machines can be observed compared to the TW-PDRPM machines.

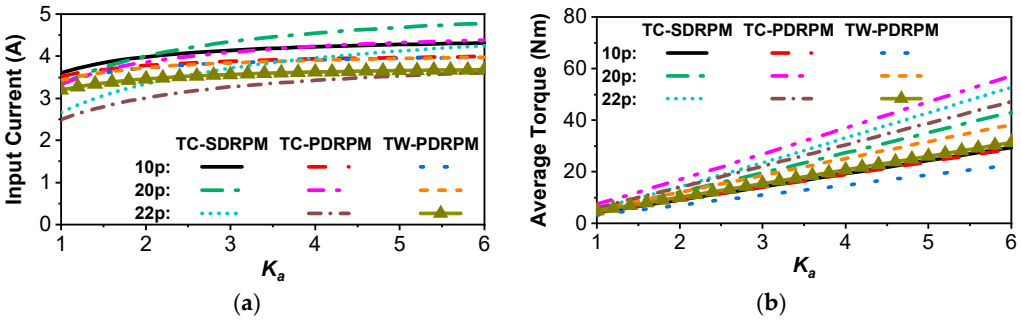

Figure 27. Variation of average torque and stator q axis input current with K_a. (**a**) Input current. (**b**) Average torque.

6.3. Scale-Up in Radial and Axial Directions

When both the radial and axial directions are scaled up, the copper loss scales up as $K_a \times K_r{}^2$. Figure 28 shows the relationships between the torque of all the machines with K_a and K_r.

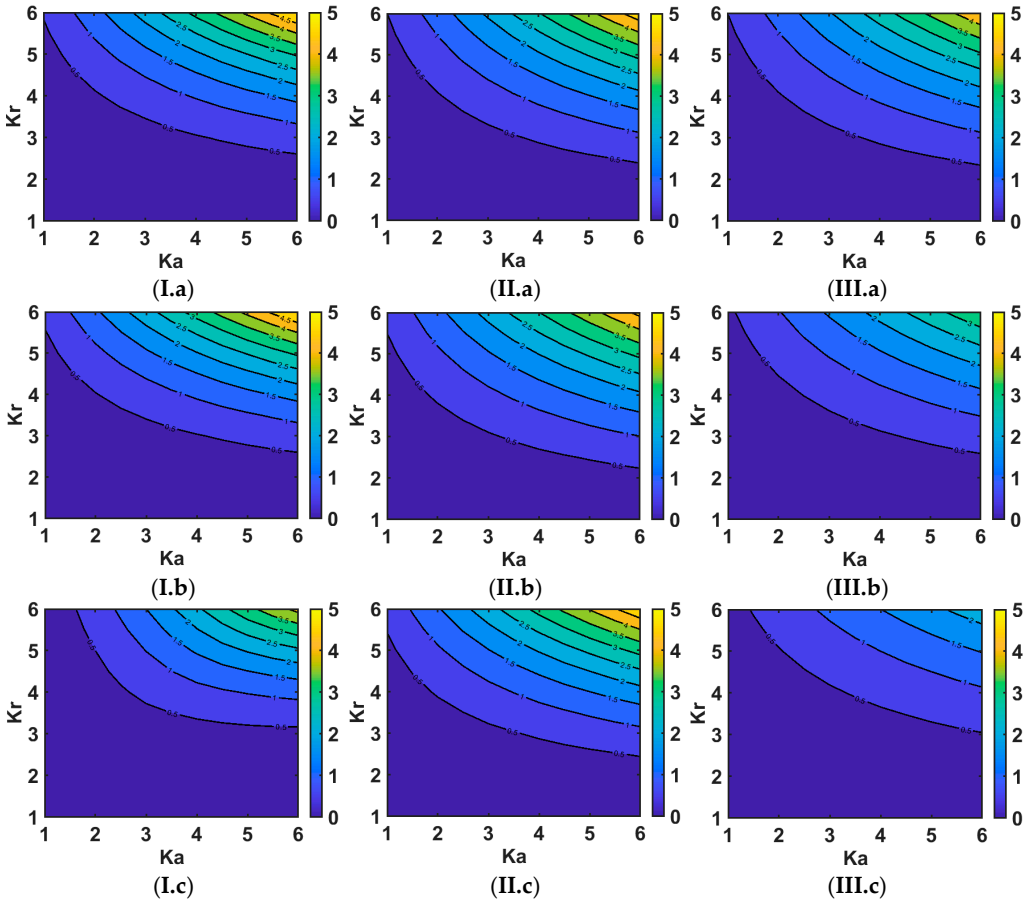

Figure 28. Variation of average torque with K_r and K_a. (**I**). 12s10p. (**II**). 12s20p. (**III**). 12s22p. (**a**) TC-SDRPM. (**b**) TC-PDRPM. (**c**) TW-PDRPM.

As mentioned in Section 6.1, the IS TW-PDRPM machines have higher stator q axis input currents than the IS TC-SDRPM and TC-PDRPM machines due to their short end-winding length. However, when the axial direction is considered. The stator q axis input current difference is insignificant compared to when only the radial direction scales up. Therefore, the advantage of the short end-winding in the TW-PDRPM machines is less. The TC-SDRPM machine performs well with different slot/pole number combinations when both the radial and axial lengths increase.

6.4. Summary

The TC-SDRPM, TC-, and TW-PDRPM machines with different slot/pole number combinations and machine sizes are discussed in this section. Figure 29 shows the recommended machine type for different machine sizes. The discussion on the applicability of the different machine types in different dimensions only considered the electromagnetic torque of the machines. It can be concluded that the TW-PDRPM machine is better for the large-radius and small-axial length application due to the short end-winding length of the TW configuration. On the other hand, the TC-PDRPM machine is suitable for large-axial length and small-radius applications due to its relatively higher torque, and the end-winding length becomes gradually negligible with the increasing axial length. The TC-SDRPM machine always performs well when both the radial and axial lengths increase.

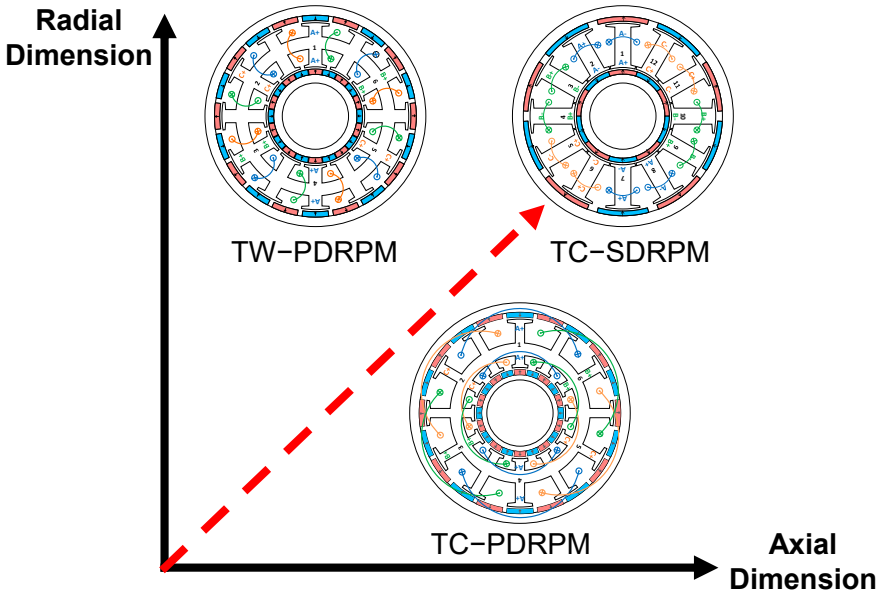

Figure 29. Recommended machine type for different machine sizes for higher torque production.

7. Experiment Validation

The 12s10p TW-PDRPM and TC-SDRPM machines (Figure 30) are prototyped and tested to validate the FEA results. The design parameters are listed in Tables 2 and 3.

The cogging torques and static torques of the 12s10p TC-SDRPM and TW-PDRPM machines are measured by using the test method in [29] and the test rig shown in Figure 31. The phase back EMFs of two machines are obtained at 800 r/min. The FEA predicted and measured results of cogging torques and back EMFs of the two machines are shown in Figures 32 and 33, respectively. Although the amplitudes and waveforms exhibit some differences, it is worth mentioning that both the FEA and experiments confirm the small cogging torques in the prototype machines. The differences between the measured and the predicted torque and EMF amplitudes are mainly attributed to the manufacturing imperfection. Overall, for both the back EMF and cogging torque, the FEA predictions are well validated by experiments.

The full and half load static torques of TW-SDRPM and TC-PDRPM machines are measured by injecting a range of DC ($I_A = -2\,I_B = -2\,I_C = I_{DC}$), and the full load current I_{rated} corresponds to the copper loss of 30 W, as shown in Figure 34a. Figure 34b shows the variation in the average torque with current. The measured torques match well with the FEA results, and as expected, the TC-SDRPM machine has a higher torque compared to the TC-SDRPM machine.

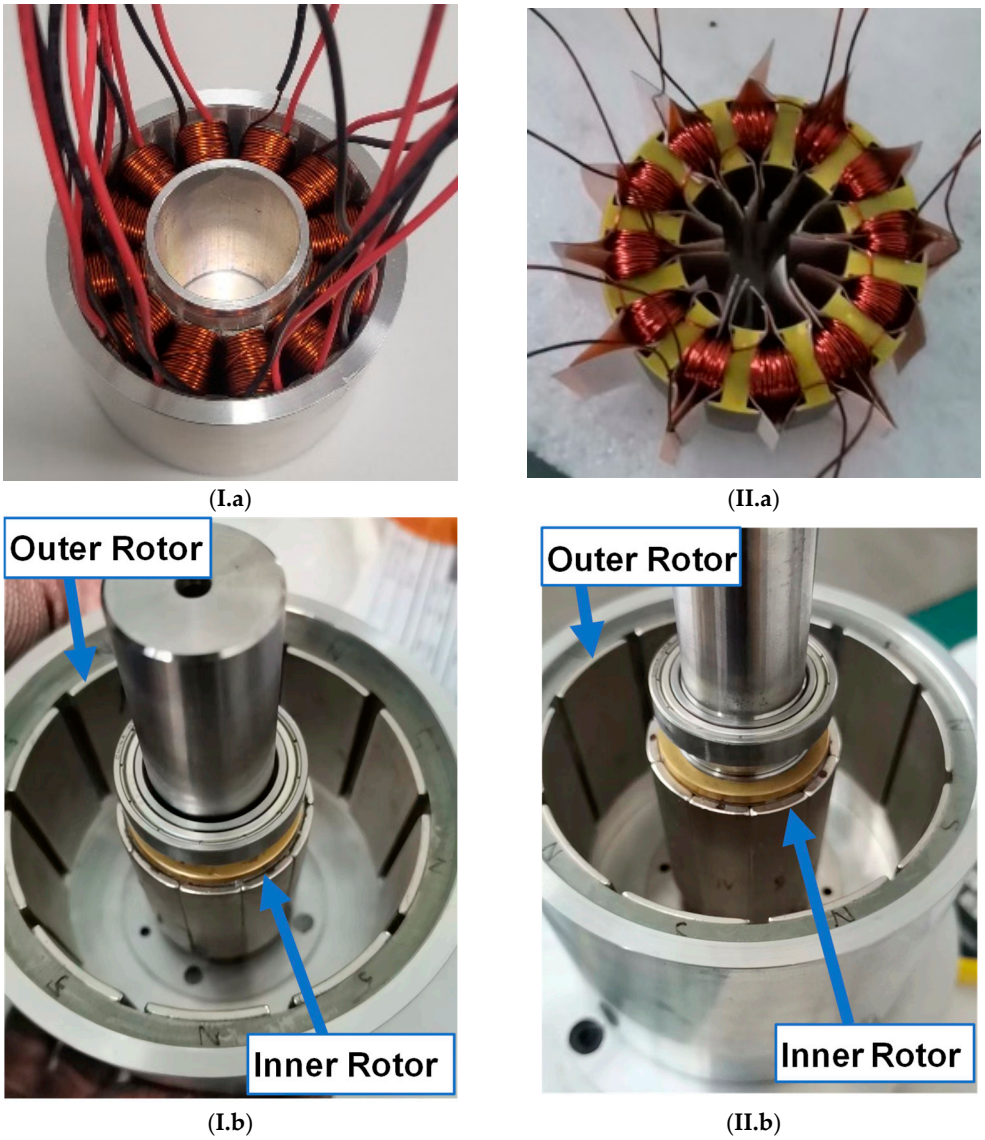

Figure 30. 12s10p machine prototypes. (**I**). TC-SDRPM. (**II**). TW-PDRPM. (**a**) Stator. (**b**) Rotor.

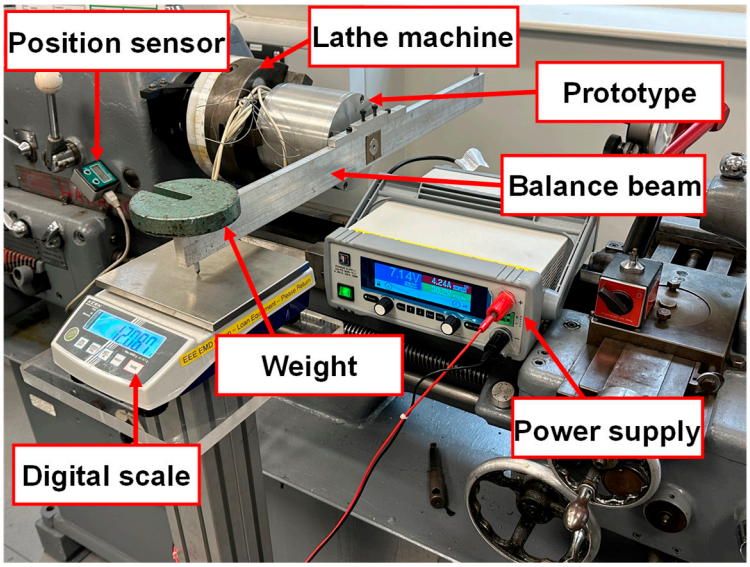

Figure 31. Test rig for static torque measurement.

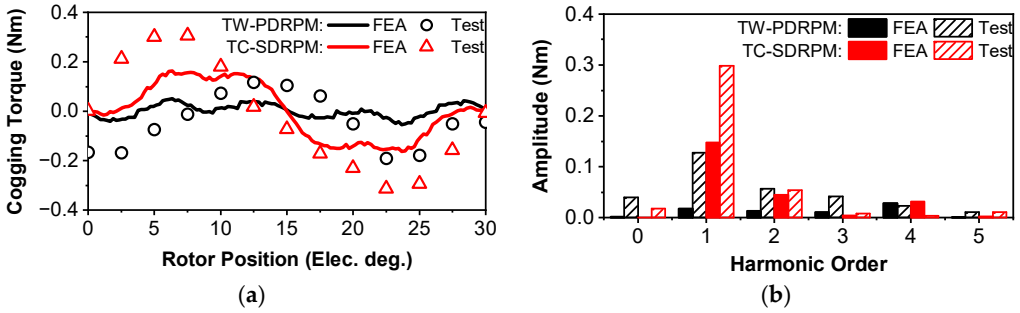

Figure 32. FEA predicted and measured cogging torques. (**a**) Waveforms. (**b**) Spectra.

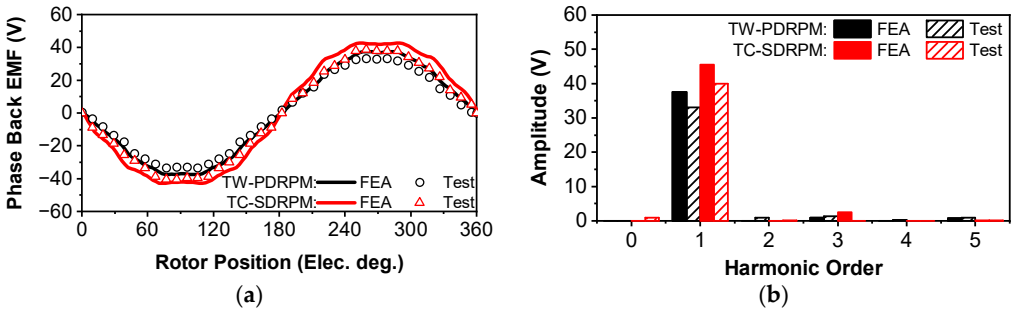

Figure 33. FEA predicted and measured phase back EMFs. (**a**) Waveforms. (**b**) Spectra.

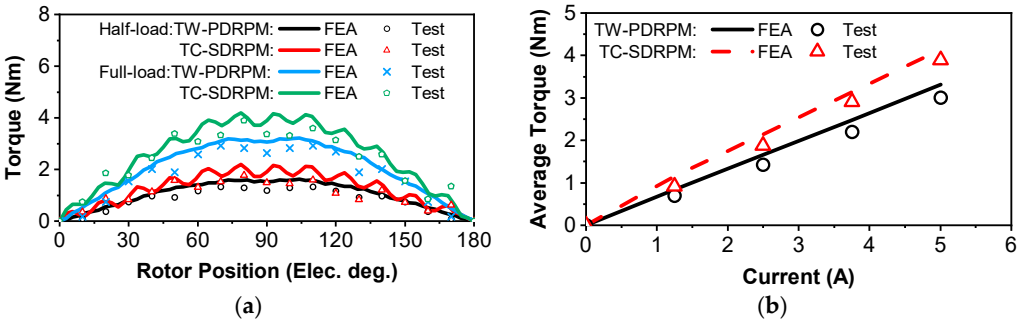

Figure 34. FEA and measured torques. (**a**) Static torques at full and half-load conditions. (**b**) Variation of average torques with currents.

8. Conclusions

This paper has presented a comparative study of radial-flux TC-SDRPM, TC-PDRPM, and TW-PDRPM machines with different slot/pole number combinations and machine sizes. All machines are optimised by the FEA genetic algorithm.

Some conclusions can be drawn as follows:

1. In a radial structure machine, the outer rotor inherently has a larger radius than the inner rotor, resulting in a larger pole arc for the outer rotor PM, producing a higher flux. The TC-PDRPM machine has the highest utilisation of the outer rotor PM. Thus, the TC-PDRPM machine has the highest PM utilisation among all types of machines with different slot/pole number combinations.
2. In terms of machine size scaling effects, the 12s20p TW-PDRPM machine shows the highest torque when scaling up radially, which is attributed to its short end-winding. The 12s20p TC-PDRPM machine performs better in axial scaling up, since the TC-PDRPM machine has the highest torque, and the end-winding length is negligible with the axial length increase. The TC-SDRPM machine has the best performance when the machine scales up in both the axial and radial directions.

The 12s10p TW-PDRPM and TC-SDRPM machines have been prototyped for validation. The experimental results have good agreement with the FEA.

Author Contributions: Conceptualization, methodology, software, validation, formal analysis, and writing—original draft preparation, Z.R. and Z.-Q.Z.; supervision, Z.-Q.Z. and D.L. All authors have read and agreed to the published version of the manuscript.

Funding: This research received no external funding.

Data Availability Statement: The original contributions presented in this study are included in the article. Further inquiries can be directed to the corresponding author .

Conflicts of Interest: The authors declare no conflicts of interest.

References

1. Zhu, Z.Q.; Howe, D. Electrical machines and drives for electric, hybrid, and fuel cell vehicles. *Proc. IEEE* **2007**, *95*, 746–765. [CrossRef]
2. Polinder, H.; Ferreira, J.A.; Jensen, B.B.; Abrahamsen, A.B.; Atallah, K.; McMahon, R.A. Trends in wind turbine generator systems. *IEEE J. Emerg. Sel. Top. Power Electron.* **2013**, *1*, 174–185. [CrossRef]
3. Cao, W.P.; Mecrow, B.C.; Atkinson, G.J.; Bennett, J.W.; Atkinson, D.J. Overview of electric motor technologies used for more electric aircraft (MEA). *IEEE Trans. Ind. Electron.* **2012**, *59*, 3523–3531.
4. Pellegrino, G.; Vagati, A.; Guglielmi, P.; Boazzo, B. Performance comparison between surface-mounted and interior PM motor drives for electric vehicle application. *IEEE Trans. Ind. Electron.* **2012**, *59*, 803–811. [CrossRef]
5. Bianchi, N.; Bolognani, S.; Frare, P. Design criteria for high-efficiency SPM synchronous motors. *IEEE Trans. Energy Convers.* **2006**, *21*, 396–404. [CrossRef]
6. Reddy, P.B.; El-Refaie, A.M.; Huh, K.K.; Tangudu, J.K.; Jahns, T.M. Comparison of interior and surface PM machines equipped with fractional-slot concentrated windings for hybrid traction applications. *IEEE Trans. Energy Convers.* **2012**, *27*, 593–602. [CrossRef]
7. Qu, R.; Lipo, T.A. Dual-rotor, radial-flux, toroidally wound, permanent-magnet machines. *IEEE Trans. Ind. Appl.* **2003**, *39*, 1665–1673.
8. Qu, R.; Aydin, M.; Lipo, T.A. Performance comparison of dual-rotor radial-flux and axial-flux permanent-magnet BLDC machines. In Proceedings of the IEEE International Electric Machines and Drives Conference, Madison, WI, USA, 1–4 June 2003; IEMDC'03; Volume 3, pp. 1948–1954.
9. Xu, F.; He, T.; Zhu, Z.Q.; Wang, Y.; Cai, S.; Bin, H.; Wu, D.; Gong, L.; Chen, J. Influence of slot number on electromagnetic performance of 2-pole high-speed permanent magnet motors with toroidal windings. *IEEE Trans. Ind. Appl.* **2021**, *57*, 6023–6033. [CrossRef]
10. Hassannia, A. Conceptual design of fractional slot concentrated winding dual-rotor double-speed synchronous motor. *IEEE Trans. Energy Convers.* **2020**, *35*, 986–993. [CrossRef]
11. Si, J.; Zhang, T.; Hu, Y.; Gan, C.; Li, Y. An axial-flux dual-rotor slotless permanent magnet motor with novel equidirectional toroidal winding. *IEEE Trans. Energy Convers.* **2022**, *37*, 1752–1763. [CrossRef]
12. Xu, P.; Liu, X.; Shi, K.; Du, Y. Design of dual-rotor radial flux permanent-magnet generator for wind power applications. *Appl. Mech. Mater.* **2013**, *416/417*, 9–14. [CrossRef]
13. Ullah, W.; Khan, F.; Hussain, S.; Yousuf, M.; Akbar, S. A novel dual port dual rotor wound field flux switching generator with uniform and non-uniform rotor poles for counter-rotating wind power generation. *IEEE Trans. Energy Convers.* **2023**, *38*, 2420–2433. [CrossRef]
14. Ullah, W.; Khan, F.; Akuru, U.B.; Yousuf, M. Magnetic coupling effect and performance analysis of dual rotor permanent magnet flux switching generator for counter rotating wind power generation. *IEEE Trans. Energy Convers.* **2023**, *38*, 2895–2908. [CrossRef]
15. Potgieter, J.H.J.; Kamper, M.J. Design optimization of directly grid-connected PM machines for wind energy applications. *IEEE Trans. Ind. Appl.* **2015**, *51*, 2949–2958. [CrossRef]
16. Xu, P.; Shi, K.; Sun, Y.; Zhua, H. Effect of pole number and slot number on performance of dual rotor permanent magnet wind power generator using ferrite magnets. *AIP Adv.* **2017**, *7*, 056631. [CrossRef]
17. Allahyari, A.; Torkaman, H. A novel high-performance consequent pole dual rotor permanent magnet vernier machine. *IEEE Trans. Energy Convers.* **2020**, *35*, 1238–1246. [CrossRef]
18. van Wijk, J.H.; Kamper, M.J. Double-sided rotor technology for iron-cored permanent magnet wind generators: An evaluation. In Proceedings of the 2013 IEEE International Conference on Industrial Technology (ICIT), Cape Town, South Africa, 25–28 February 2013; pp. 1892–1897.

19. Golovanov, D.; Papini, L.; Gerada, D.; Xu, Z.; Gerada, C. Multidomain optimization of high-power-density PM electrical machines for system architecture selection. *IEEE Trans. Ind. Electron.* **2018**, *65*, 5302–5312. [CrossRef]
20. Golovanov, D.; Gerada, C. An analytical subdomain model for dual-rotor permanent magnet motor with Halbach array. *IEEE Trans. Magn.* **2019**, *55*, 8205216. [CrossRef]
21. Ran, Z.T.; Zhu, Z.Q. Comparative study of dual- and single-rotor radial-flux fractional-slot PM machines. *IEEE Access* **2024**, *12*, 147709–147722. [CrossRef]
22. Jian, L.; Gong, W.; Xu, G.; Liang, J.; Zhao, W. Integrated magnetic-geared machine with sandwiched armature stator for low-speed large-torque applications. *IEEE Trans. Magn.* **2012**, *48*, 4184–4187. [CrossRef]
23. Potgieter, J.H.J.; Kamper, M.J. Double PM-rotor, toothed, toroidal-winding wind generator: A comparison with conventional winding direct-drive pm wind generators over a wide power range. *IEEE Trans. Ind. Appl.* **2016**, *52*, 2881–2891. [CrossRef]
24. Ran, Z.; Zhu, Z.Q.; Liang, D. Comparative study of radial-flux dual-rotor fractional-slot permanent magnet machines with series and parallel magnetic circuits. In Proceedings of the 2022 25th International Conference on Electrical Machines and Systems (ICEMS), Chiang Mai, Thailand, 29 November–2 December 2022; pp. 1–6.
25. Zhu, Z.Q. Fractional slot permanent magnet brush-less machines and drives for electric and hybrid propulsion systems. *Compel* **2011**, *30*, 9–31. [CrossRef]
26. EL-Refaie, A.M. Fractional-slot concentrated-windings synchronous permanent magnet machines: Opportunities and challenges. *IEEE Trans. Ind. Electron.* **2010**, *57*, 107–121. [CrossRef]
27. He, T.R.; Zhu, Z.Q.; Xu, F.; Bin, H.; Wu, D.; Gong, L.M.; Chen, J.T. Comparative study of 6-slot/2-pole high-speed permanent magnet motors with different winding configurations. *IEEE Trans. Ind. Appl.* **2021**, *57*, 5864–5875. [CrossRef]
28. Xu, F.; Zhu, Z.Q.; He, T.R.; Wang, Y.; Bin, H.; Wu, D.; Gong, L.M.; Chen, J.T. Influence of stator gap on electromagnetic performance of 6-slot/2-pole modular high speed permanent magnet motor with toroidal windings. *IEEE Access* **2021**, *9*, 94470–94494. [CrossRef]
29. Zhu, Z.Q. A simple method for measuring cogging torque in permanent magnet machines. In Proceedings of the 2009 IEEE Power & Energy Society General Meeting, Calgary, AB, Canada, 26–30 July 2009; Volumes 26–30; pp. 1–4.